SCIENCE CHINA
Earth Sciences

• RESEARCH PAPER •

April 2012 Vol.55 No.4: 590–601
doi: 10.1007/s11430-011-4259-1

Landslide monitoring with high-resolution SAR data in the Three Gorges region

LIAO MingSheng*, TANG Jing, WANG Teng, BALZ Timo & ZHANG Lu

State Key Laboratory of Information Engineering in Surveying, Mapping and Remote Sensing, Wuhan University, Wuhan 430079, China

Received June 24, 2010; accepted March 22, 2011; published online December 15, 2011

Employing the well-known D-InSAR technique, we investigated landslide monitoring in the Three Gorges region using TerraSAR-X data. The experiment demonstrates that using both the amplitude and differential phase allows us to identify the precise location, deformation and time range of occurrence of certain landslides. To overcome the atmospheric effect on D-InSAR results, a time-series analysis was also carried out. The observed nonlinear relationship between the deformation and water level suggests that reservoir water level fluctuation is one of the major causes of landslides, which is significant in terms of issuing landslide warnings. In addition, the comparison of TerraSAR-X and C-band ASAR data results indicates that TerraSAR-X data provide far more reasonable deformation measurements because of their high temporal and spatial resolutions.

landslide monitoring, D-InSAR, time series analysis, high resolution

Citation: Liao M S, Tang J, Wang T, et al. Landslide monitoring with high-resolution SAR data in the Three Gorges region. Sci China Earth Sci, 2012, 55: 590–601, doi: 10.1007/s11430-011-4259-1

A landslide refers to rock mass sliding along a rupture plane, which may be caused by natural or anthropic factors [1]. As a common geological disaster, landslides are widely distributed and often greatly endanger the safety and property of nearby residents. Statistical results for 2009 indicate that landslides account for more than 60% of all geological disasters in China. The occurrence of landslides depends on the actions of both intrinsic and external factors. Intrinsic factors largely relate to geological structure and topographic features, such as stratal lithology and topographical relief. External factors such as earthquakes, rain and human construction are the main causes of large landslides.

The Three Gorges Project, located at Sandouping near Yichang, Hubei Province, is the largest hydroelectric project in the world. The Three Gorges Project has greatly benefited flood control, power generation and navigation capability. With implementation of the project, the up-river water level rose 100 m to a new level of 175 m. Moreover, the river levels vary from 145 to 175 m during each store-release cycle, and the reservoir surroundings are thus at high risk of geological disasters [2].

In a 2001 statistical survey carried out by the Ministry of Land and Resources of China, landslides were observed in all counties surrounding the Three Gorges reservoir; nearly 2500 landslide bodies were observed. However, when the river level reached 135 m in November 2003, the number of landslide bodies and bank collapses had reached 4688, nearly double the number in 2001. According to a report given at a Three Gorges reservoir geological disaster protection meeting in June 2010, there have been 132 geological disasters since 2009, and more than 2000 people have had to be relocated.

Zigui County is one area in the Three Gorges region that is seriously affected by geological hazards. The county and its surrounding area have many landslide bodies with poor

*Corresponding author (email: liao@whu.edu.cn)

slope stability. After the impoundment of the Three Gorges reservoir in June 2003, there has been much focus on the instability and reactivation of old landslides [3]. The Qianjiangping landslide presents the most serious risk during a phase of storing water. It was preliminary concluded that rising water and continuous heavy rain are the main factors involved in reactivating the old Qianjiangping landslide body [4].

Nowadays, various methods are jointly used to monitor the deformation of landslides in the Three Gorges region, such as geodesic measurement, implementation of a monitoring network based on the global positioning system, and interpretation of remote-sensing images. The Yangtze River Three Gorges landslide monitoring station was established for long-term deformation monitoring of Xintan-Lianziya landslide bodies close to the dam. Although these methods obtain highly accurate results, they do not easily obtain a high density of measurement points because of manpower and instrumentation costs.

As an active microwave sensor, the Synthetic Aperture Radar (SAR) is especially suitable for cloudy and rainy areas such as the Three Gorges region [5]. With prior knowledge of topography, millimeter deformation can be detected from two images acquired at different times. The so-called differential interferometric SAR (D-InSAR) technique can acquire ground deformation at a large scale and has thus been widely researched for several applications such as the monitoring of earthquake, volcanic and mining deformations [6–8]. In 1996, Fruneau et al. [9] attempted to employ the D-InSAR technique to monitor the Saint Etiennede Tin landslide in southern France, and they found that the results agreed well with ordinary measurements.

However, more thorough investigations of D-InSAR showed that its application is limited for several reasons: (1) spatial decorrelation due to large normal baselines, (2) temporal decorrelation due to surface changes at different acquisition times, (3) atmospheric phase screening (APS) due to different water vapor levels, and (4) systematic thermal noise, data processing errors and other errors.

In 1999, Ferretti et al. [10, 11] at Politecnico di Milano (POLIMI) proposed the permanent scatterers InSAR (PS-InSAR) technique, which focuses on stable point-like targets (PSs), to improve the accuracy of the deformation measurement. On the basis of a natural network constructed with PS points, phases dependent on terrain, deformation and atmosphere can be separated from each other according to their different spatial and temporal characteristics. Thus, a highly accurate deformation result can be achieved for the PS network. A series of relative techniques, such as coherent target analysis and spatial-temporal phase unwrapping, have been presented to extend D-InSAR application 12. The PS-InSAR technique advances D-InSAR and has been successfully applied in many cases of monitoring ground deformation 13,14. Meanwhile, the Stanford group presented their time-series InSAR analysis method—the Stanford method for persistent scatterer (StaMPS). StaMPS employs a three-dimensional phase unwrapping technique instead of a prior deformation model to measure target deformation [15, 16].

In 2000, the PS technique was employed to monitor Ancona landslide deformation in Italy. The measurements obtained from the InSAR datasets were consistent with the ground truth. The accuracy of the deformation velocity reached a millimeter level [11]. In 2003, Colesanti et al. [17] processed 61 scenes of Europe Remote-Sensing Satellite (ERS) SAR images acquired from 1992 to 2001 around an Acona landslide and compared the results with leveling survey measurements; the results demonstrated the capability of the PS technique, and good agreement was even found in low-coherence areas covered by plants. In 2006, Hilley et al. [18] pointed out that landslide deformation was related to rainfall by analyzing a nonlinear deformation series obtained from InSAR data.

In 2001, the Geophysics Institute of Alaska University and the National Seismological Bureau of China launched a joint deformation monitoring project in the Three Gorges region using ERS data provided by the European Space Agency (ESA). However, the results were not as good as anticipated because of the high decorrelation due to vegetation and steep terrain in this region [19]. Gao et al. [20] carried out a time-series InSAR analysis with 11 scenes of ASAR data taken over Wanzhou. The results showed that the limited number of images and strong APS distribution limited the InSAR application in this region. With the support of the ESA-NRSCC Dragon Program, Wuhan University and POLIMI worked together to carry out a ground subsidence study over the area of the Three Gorges Project and Badong. The time-series InSAR analysis indicated that the dam body only has slight deformation due to differing water levels and temperatures, while two slowly moving landslide areas were identified in Badong [21–23].

Before 2008, ERS and ENVISAT ASAR C-band mid-resolution images with a 35-day revisiting period were the main data sources for InSAR applications. In such investigations, because of their low resolution, it was difficult to refine the analysis of a certain landslide body even using partially coherent targets to improve the measurement density [23]. Since 2007, a series of SAR satellites with high resolutions and shorter revisiting times have been launched, such as the TerraSAR-X and COSMO-SkyMed systems [24]. Better InSAR results are expected using images with both higher spatial and temporal resolution [25, 26], and we therefore focus on landslide monitoring in the Three Gorges region using TerraSAR-X data in this paper. The experiment results show that the high-resolution InSAR image stack is valuable in landslide monitoring and the early warning of disasters.

1 D-InSAR/time-series InSAR techniques

1.1 D-InSAR technique

The major steps in D-InSAR data processing are the input of master and slave images, subtraction of the flat-Earth effect and phase unwrapping. In general, according to the number of images used in D-InSAR data processing, there are three methods for subtracting topography-dependent phases. The first obtains deformation phases directly from the image pair with a zero baseline. The second simulates topographic phases with an external digital elevation model (DEM) and then subtracts them from the interferogram. The above methods use only two InSAR images, but a zero-baseline image pair and a good external DEM are usually difficult to find [6]. The third method obtains topographic phases from a pair of InSAR images with a long spatial but short temporal baseline, and then measures the deformation from another interferogram by subtracting the unwrapped topographic phases. This method requires three or four interferograms, and phase unwrapping has to be carried out [7].

1.2 Time-series InSAR analysis

The time-series InSAR analysis technique incorporates numerous SAR images of the same area and then identifies persistent scatterers through statistical analysis of their amplitudes and phases. The PS points make up of a "natural monitoring network", on which the APS dependence can be obtained by fitting the phases. After subtracting the APS effect, the deformation monitoring accuracy is improved considerably.

Compared with the traditional D-InSAR technique, the superiorities of time-series InSAR are: (1) point-like targets meet the requirement of high coherence for D-InSAR processing, (2) because the baseline restriction can be loosened, more images can be used, (3) the statistical analysis of APS reduces the main error source in deformation monitoring, and (4) an external DEM with low accuracy can be used to subtract the topographic phase because the elevation of PS points is refined later.

Although time-series InSAR analysis opens up the possibility for long-term measurement of slowly progressing and tiny deformations, many SAR images need to be acquired, which is the main disadvantage of this technique.

In urban areas, ground subsidence can be assumed as a linear change with time, and thus, original PS processing can provide good results [14]. However, landslide deformation, which is related to heavy rainfall and human activity, is often complicated to model. In addition, because landslides are usually in non-urban areas where there are fewer man-made targets and few PS candidates can be identified from the deviation in their amplitude series. As a consequence, the time-series InSAR analysis for monitoring landslide deformation is usually carried out as follows [15, 23].

(1) Differential interferometry. One "master" image is chosen from $N + 1$ images and then N differential interferograms are produced after coregistration. The differential phase can be written as

$$f_p^{i,k} = f_S^{i,k} + f_B^{i,k} + f_T^{i,k} + f_N^{i,k}, \quad (1)$$

where $f_p^{i,k}$ denotes the differential phase of P for interferogram i; $f_S^{i,k}$ denotes the spatially related phase, including the atmospheric phase, orbit error, DEM error and surface deformation; $f_B^{i,k}$ refers to the phase that correlates with the perpendicular baseline; $f_T^{i,k}$ refers to the temporally related phase resulting from spatially uncorrelated surface deformation and seasonal variation in the atmospheric phase; and $f_N^{i,k}$ is the noise phase.

(2) PS candidates are initially selected on the basis of amplitude dispersion.

(3) Filtering $f_S^{i,k}$. All PS candidates are transformed to a regular grid with spacing over which little variation in phase is expected after geocoding. As this term is correlated with in certain space and has low frequency, $f_S^{i,k}$ can be subtracted using a low-pass filter with a typical cutoff wavelength in the range from 800 to1200 m [27].

(4) $\tilde{f}_B^{i,k}$ is estimated by linear inversion from both the residual phase and perpendicular baseline. After subtracting the spatially correlated phase, the non-spatially correlated phases of deformation, atmosphere and orbit error are very small and the baseline-related phase is dominant. Because the phase is wrapped, the parameter space is searched to estimate the phase. We typically limit the rough search to a height error of ±10 m and increments such that the range is π/4. When x_B reaches its maximum value, $\tilde{f}_B^{i,k}$ is assigned as the optimal value.

$$x_B = \frac{1}{M}\sum_{i=1}^{M}\exp\{j(f_p^i - \tilde{f}_{Sp}^i - \tilde{f}_{Bp}^i)\}, \quad (2)$$

where x_B is a measure of the phase noise level and an indicator of whether the pixel is a PS and M denotes the number of interferograms. Once the value of x_B is known, we can select persistent scatters combining both amplitude and phase stability and subtract $\tilde{f}_B^{i,k}$ from differential interferograms.

On the basis of features of time-series image data, the three-dimensional spatial and temporal unwrapping method overcomes the restrictions of the predefined deformation model. By filtering the unwrapped phase, we obtain an accurate deformation phase.

1.3 Superiority of TerraSAR-X data in deformation measurement

TerraSAR-X is a new-generation German Earth-observation

satellite, the main payload of which is a high-resolution X-band (wavelength 3.1 cm) SAR. TerraSAR-X can provide a multi-mode, multi-polarization and multi-resolution SAR image for commercial and scientific use. The satellite was launched on June 15, 2007 and has been in operation since January 2008 providing precise attitude and orbit parameters [24].

In theory, because the wavelength of the X-band is nearly half that of the C-band, the X-band SAR interferogram is more sensitive to deformation signals and thus provides more accurate results. Additionally, the shorter revisiting period and higher resolution of the TerraSAR-X images allow us to obtain more deformation detail than we can obtain from mid-resolution images. In time-series InSAR analysis, because a PS often corresponds to a scatterer that dominates the echo signals within a SAR resolution cell, it is more possible to detect a PS from high-resolution data. In other words, with higher resolution, the possibility that a single scatterer dominates the radar echo within a resolution cell is also higher; therefore, we expect to obtain more PSs from the high-resolution SAR image stack [28].

Nevertheless, comparing with C- and L-band data, X-band data suffer more severe temporal decorrelation because of the higher phase sensitivity. Despite that, with the development of sensor platforms and a shorter revisiting period, temporal decorrelation can be reduced for two images acquired proximately. Furthermore, phase unwrapping is more difficult in the case of the X-band interferogram, and it is thus necessary to carry out a consistency test especially, for areas of low coherence [28].

2 Test sites and datasets

Zigui County in Yichang, Hubei Province, is located at the transition from the second to third topographic step of China. In this area, the east Sichuan fold joins the western Hubei Mountains and there are widely distributed erosion canyon landscapes. The terrain here becomes lower from east to west, as shown in Figure 1. The DEM for the test site shows that the terrain is that of low to mid-height mountains and the surface undulates with elevation ranging from 0 to 3000 m. From a geological point of view, the test site is on the Huangling anticline and Zigui synclinal and the stratum is from the Jurassic system to Silurian system from east to west [2].

In this work, we collected 57 scenes of ASAR images acquired from 2003 to 2009 and 22 scenes of TerraSAR-X SM mode images acquired from 2008 to 2009 to monitor several landslides around Zigui. The coverage of these two datasets is shown in Figure 1. Table 1 compares the basic parameters of the two sensors.

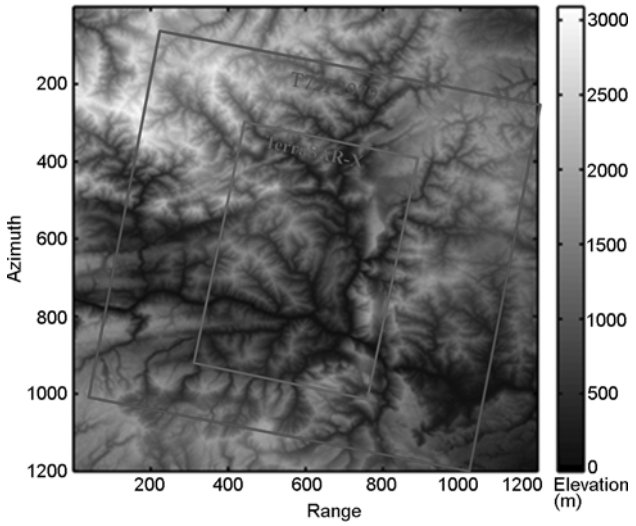

Figure 1 DEM of test sites and coverage areas of datasets.

Table 1 Basic parameters of test datasets

	ASAR data	TerraSAR-X data
Frame/Track No.	T75F2979	strip_005
Track	ascending	descending
RPF (Hz)	1652	3611
Look angle (°)	23	25
Polarization	VV	VV
Azimuth spacing (m)	4	2
Range spacing (m)	8	1
Coverage of scene	109 km × 104 km	30 km × 50 km
Wavelength (m)	0.056	0.031
Revisit cycle (d)	35	11

3 Results and discussions

3.1 D-InSAR analysis

To compare the coherence between the ASAR and TerraSAR-X datasets, two interferograms from corresponding image pairs are shown in Figures 2 and 3. The images were acquired in the same season in 2009 to reduce the temporal decorrelation difference, interferometric parameters are as shown in Table 2. In the ASAR interferogram in Figure 2, clear fringes representing high coherence are only observed around towns with man-made buildings; for instance, Guizhou marked by the red circle. We do not see visible fringes near other places. However, in Figure 3, clear fringes are seen for almost all landslide bodies. According to the interferometric phases, there is no obvious deformation for Xintan, Huangyangpan and Baishuihe landslides. In addition, coherence of corner reflectors installed near Xintan in the TerraSAR-X interferogram is much higher than that for ASAR images. The high coherence of the TerraSAR-X interferogram can be explained by its high spatial resolution. In the following, we jointly use the amplitude and phase

Table 2 D-InSAR images parameters over Zigui

ASAR data	Acquisition date	Water level (m)	Temporal baseline (d)	Perpendicular baseline (m)
Master image	2009-11-08	170.85	70	–41.6
Slave image	2009-08-30	146.32		
TerraSAR-X data	**Acquisition date**	**Water level (m)**	**Temporal baseline (d)**	**Perpendicular baseline (m)**
Master image	2009-11-06	170.87	55	–22.9
Slave image	2009-09-12	145.26		

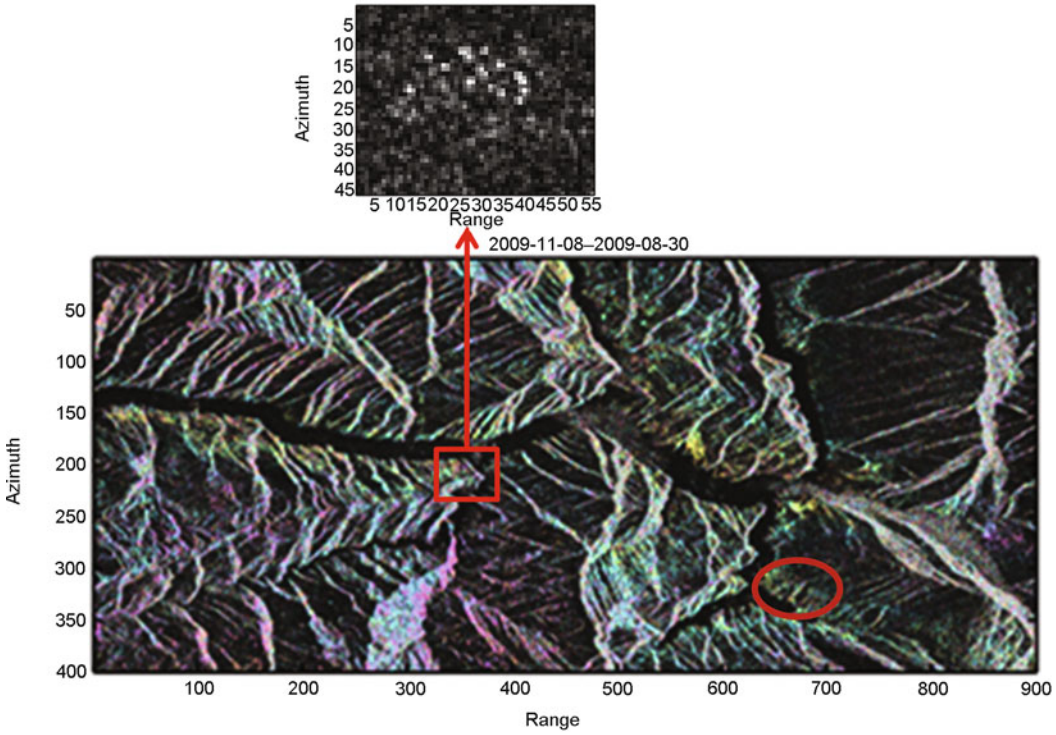

Figure 2 Differential interferogram of ASAR (the small figure above indicates Shuping with corner reflectors).

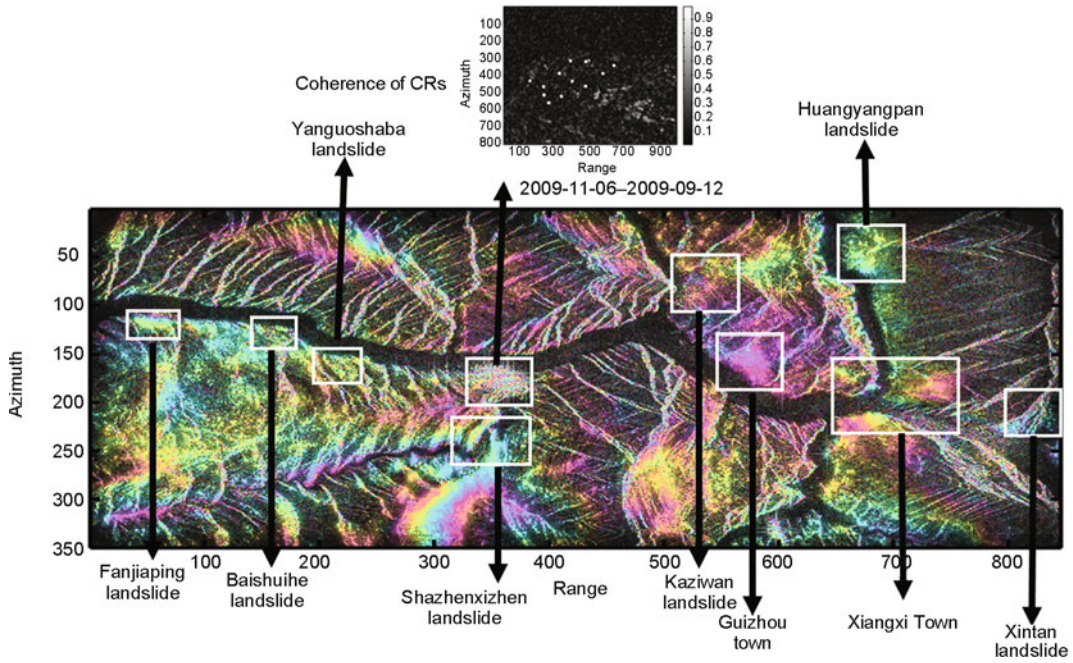

Figure 3 Differential interferogram of TerraSAR-X (the small figure above indicates Shuping with corner reflectors).

information to determine the time range of occurrence, location and deformation of a certain landslide body.

In the time-series amplitude maps shown in Figure 4, evidence that a landslide occurred can be observed easily (within the red frame). According to the acquisition time of the SAR images, the discovered landslide is consistent with a landslide that occurred on August 30, 2008. To analyze the deformation before and after the landslide, two interferograms are generated separately with images acquired on July 21 and August 3 and September 14 and October 17. The spatial baselines are –31.7 and 20.7 m respectively.

Figure 5 shows large deformation only before the landslide occurred. The blue square shows a cliff produced by the Qianjiangping landslide in 2003, and it presents as an off-white color in amplitude and obvious fringes in the differential interferogram. The dense fringes are due to the lack of an updated external DEM.

3.2 Results from time-series InSAR analysis

3.2.1 ASAR results

Here, 36 scenes ASAR images taken from November 2004 to December 2008 are used to carry out time-series analysis for an area covering 2350 pixel × 640 pixel. The spatial and temporal baselines with respect to the master image indicated by a red circle are shown in Figure 6.

Only 587 PSs are identified after processing, and the PS density is less than 5 per square kilometer. Moreover, because very few targets remain stable during the image acquisition span, the number of detection PSs decreases if more images are used for the time-series InSAR analysis. The low PS density reduces the accuracy of measurements especially for complex topography and severe atmospheric effects in this region. As we have found, higher spatial resolution leads to a higher possibility of detecting a PS. Because there are very few PSs at our test site, a possible solution is to take images with new-generation satellites. On the other hand, the detectable deformation velocity is inversely proportional to the revisiting period, and only slow deformation can be measured from the images with a long temporal baseline; therefore, it is difficult to precisely obtain fast landslide deformation from the available ASAR datasets. With higher spatial and temporal resolution (Table 1), the TerraSAR-X images meet the demands of nonlinear deformation monitoring and are particularly useful in our case of the Three Gorges region [25]. In the following discussions, our results are obtained by analyzing the TerraSAR-X datasets.

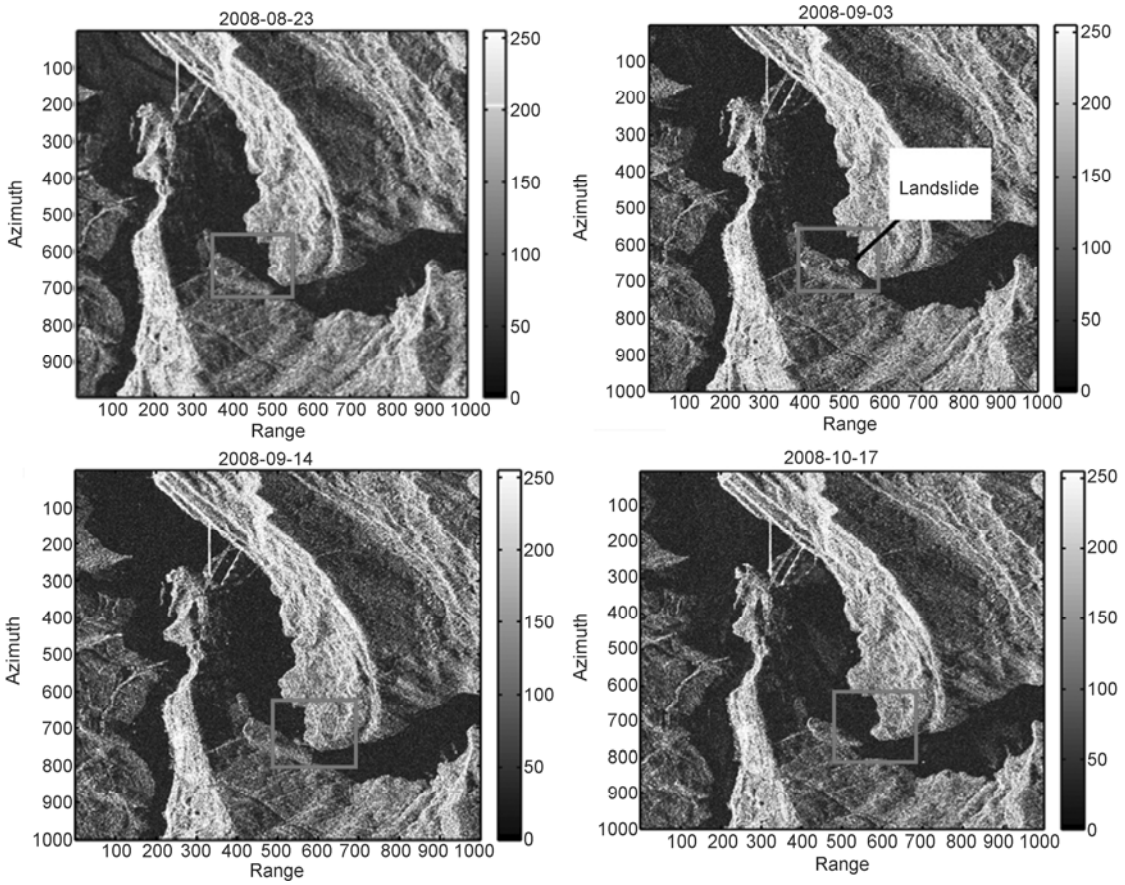

Figure 4 Amplitude variance in Shazhenxi Town before and after landslide. Water level: 145.8 m.

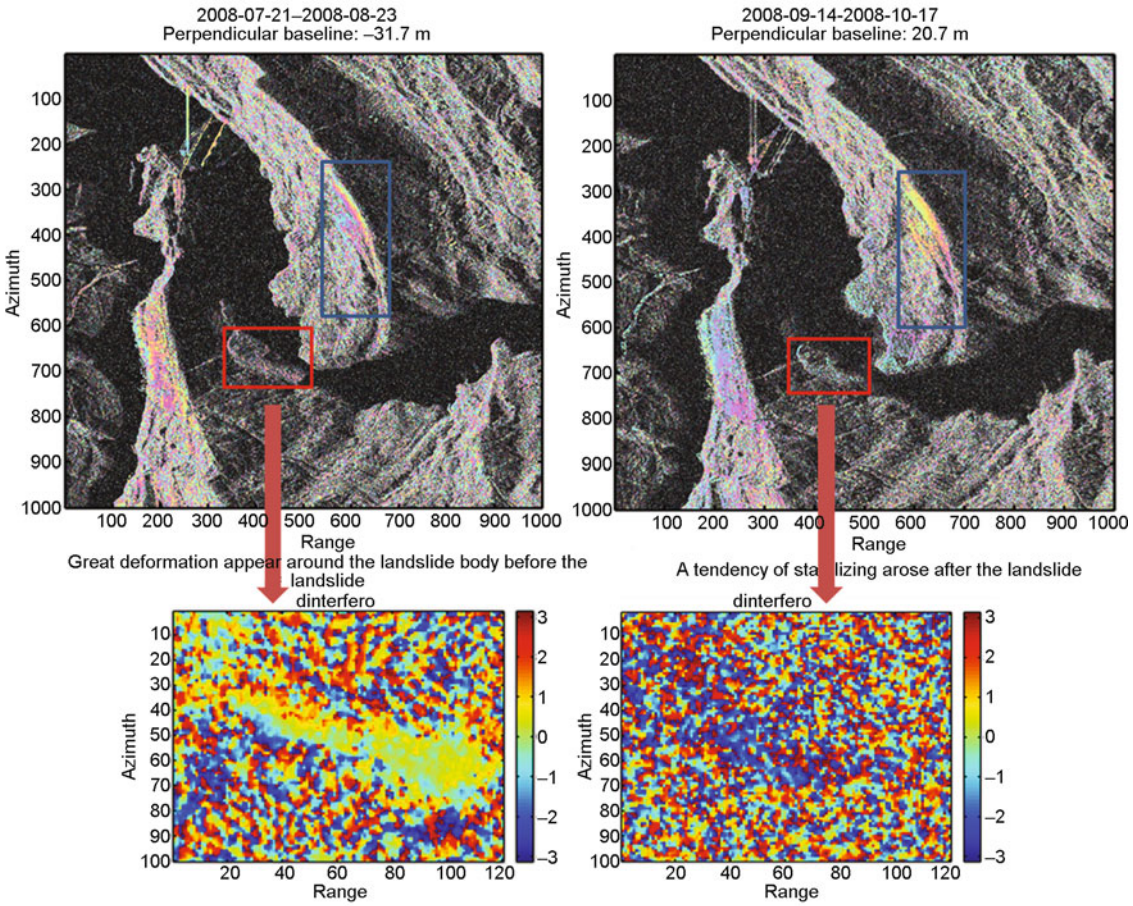

Figure 5 Deformation phase before and after landslide. (a) Differential phase before landslide; (b) differential phase after landslide.

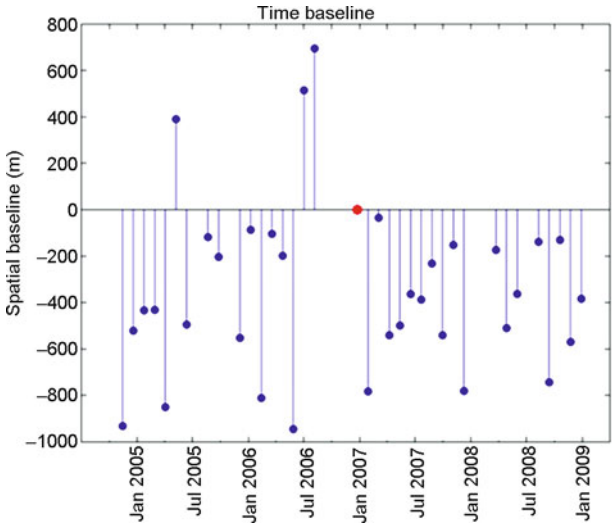

Figure 6 Spatial and temporal distribution of ASAR datasets

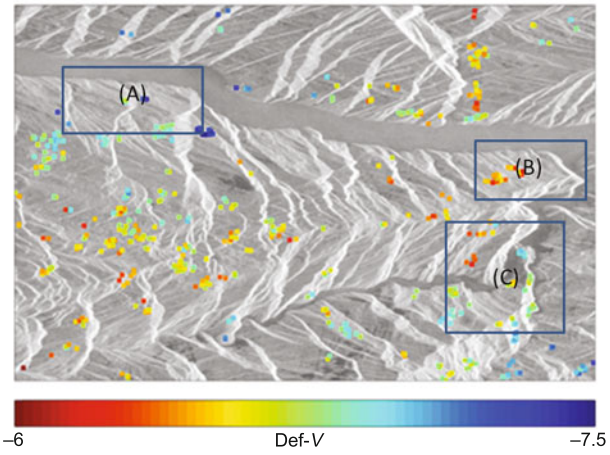

Figure 7 Deformation rate of PSs in the line of sight (mm/a).

3.2.2 TerraSAR-X results

Taking the same test site as for the ASAR datasets, this section focuses on Shuping, Baishuihe and Qingganhe, labeled (A), (B), and (C) respectively in Figure 7.

The ancient Shuping landslide is located in the town of Shazhenxi on the right bank of the Yangtze River. The landslide body looks like a round-backed armchair and the elevation ranges from 65 to 500 m. The width and length of the landslide are about 800 and 700–900 m respectively, and the toe of the landslide is under water and the elevation of the landslide shear crack is around 65–68 m. The estimated thickness of the sliding mass is 40 to 70 m. The esti-

mated total volume is around 2.600×10^7 m^3. The topography of the landslide body is gentle at top and steep at bottom, and the slope angles from 22° and 35° .

Totally, 633 PSs are identified after processing, and the PS density is about 40 per square kilometer, which meets the requirements of time-series InSAR analysis. The Shuping landslide deformation monitoring results are shown in Figure 8(a), where different colors of the points represent different deformation velocities. Most of the measured points show deformation trends of less than 2 mm/a, meaning that the Shuping landslide is quite stable. Nevertheless, by exploiting the displacement series of each image, we find that the nonlinear movements of the detected targets are strongly related to the different levels of the Yangtze River (Figure 8 (b)). The Three Gorges area has humid subtropical climate, with rainfall mainly in July and August, when there are frequent geological hazards, such as the Qianjiangping landslide. Deformation of the Shuping landslide, as an ancient landslide, has been detected from the first water reservoir June 2003, and there has been no large-scale human activity in the area since. Therefore, Figure 8 shows that the deformation series and water level series are strongly related. For example, in period I, the rapidly changing water level caused a huge deformation of up to 11.3 mm, whereas in period II, the deformation became smooth with the stabilizing of the water level. Our results show that a rapidly changing water level is an important factor of deformation. In period III, the scouring force due to the falling water level reduced the river bank uplift pressure, and significant deformation is thus observed from the time-series InSAR analysis results. Moreover, because the level of underground water inside the landslide body fell more slowly than the level of river water, the water presser differed inside and outside the landslide body, thus forcing rocks and causing strong deformation. The results shown in Figure 8(b) prove that the changing water levels in the Three Gorges reservoir partially lead to activity of the landslide bodies [29].

Baishuihe landslide is located near Baishuihe, Shazhenxi on the southern bank of the Yangtze River, and is 56 km

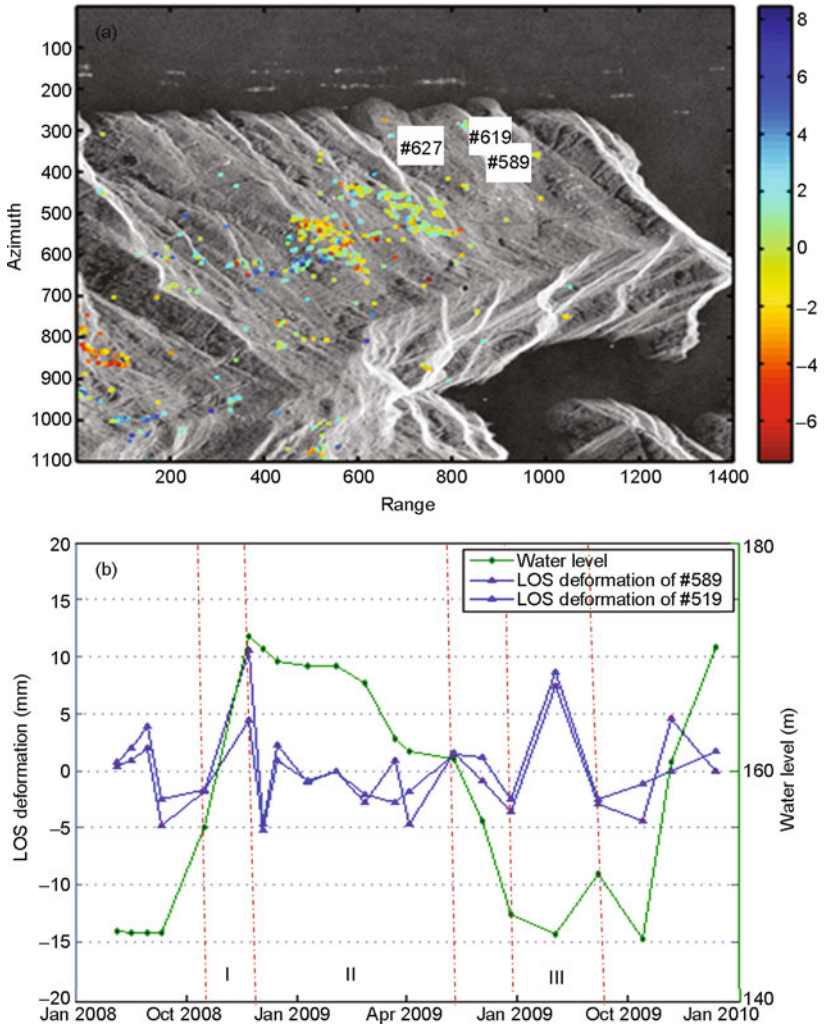

Figure 8 (a) Deformation rate of PSs in the line of sight in Shuping (mm/a); (b) nonlinear deformation analysis.

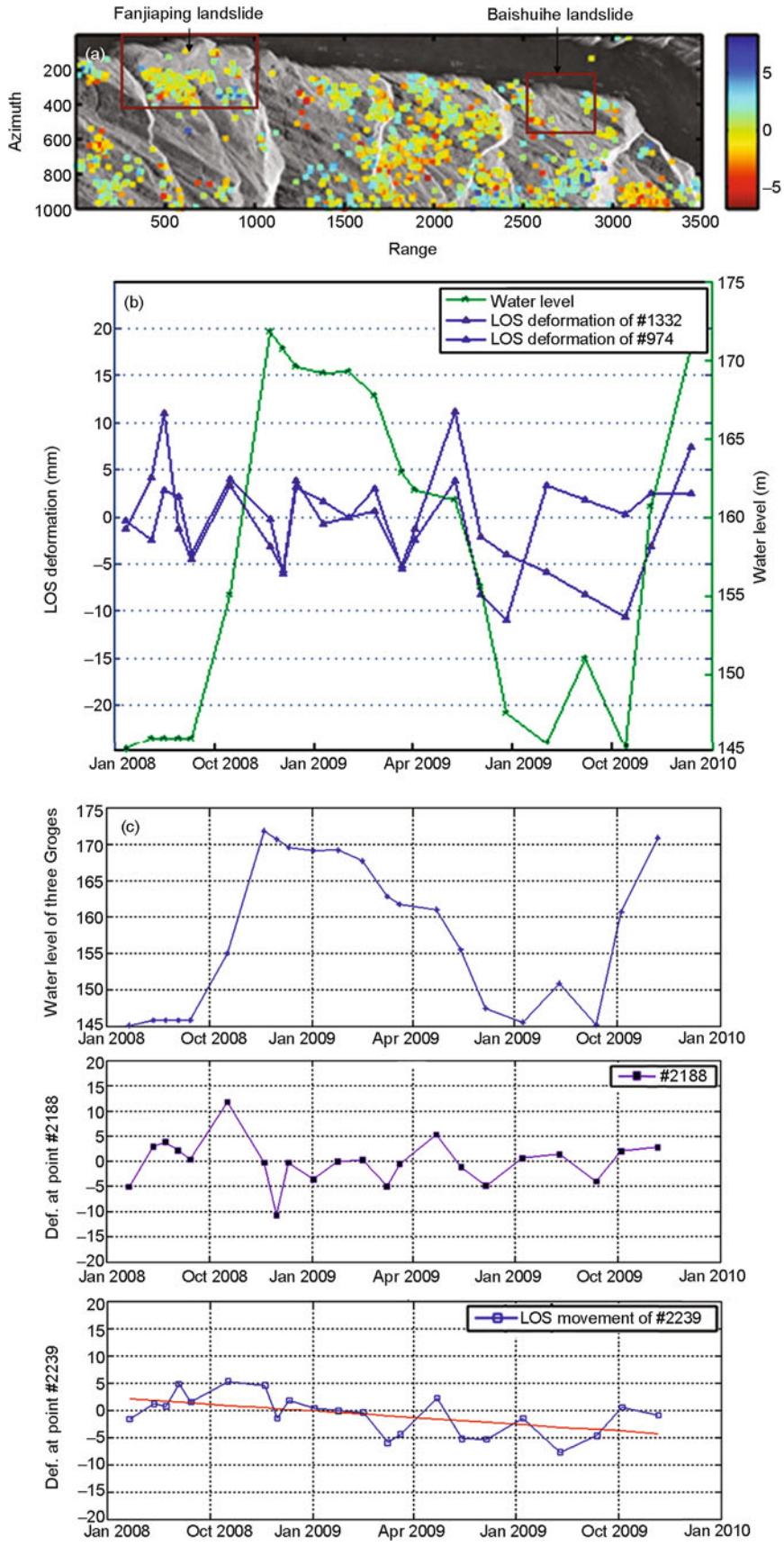

Figure 9 (a) Deformation rate of PSs in the line of sight (mm/a); (b) nonlinear deformation analysis of the Baishuihe area; (c) nonlinear deformation analysis of the Fanjiaping landslide body.

from the dam to the west. It presents toward the Yangtze River, and is located in a wide river valley, for which the geology type is monoclinal stratum and the topography is high in the north and low in the south. The sliding mass is distributed towards the river in a series of steps. The elevation of the back edge of the sliding mass is 410 m and the

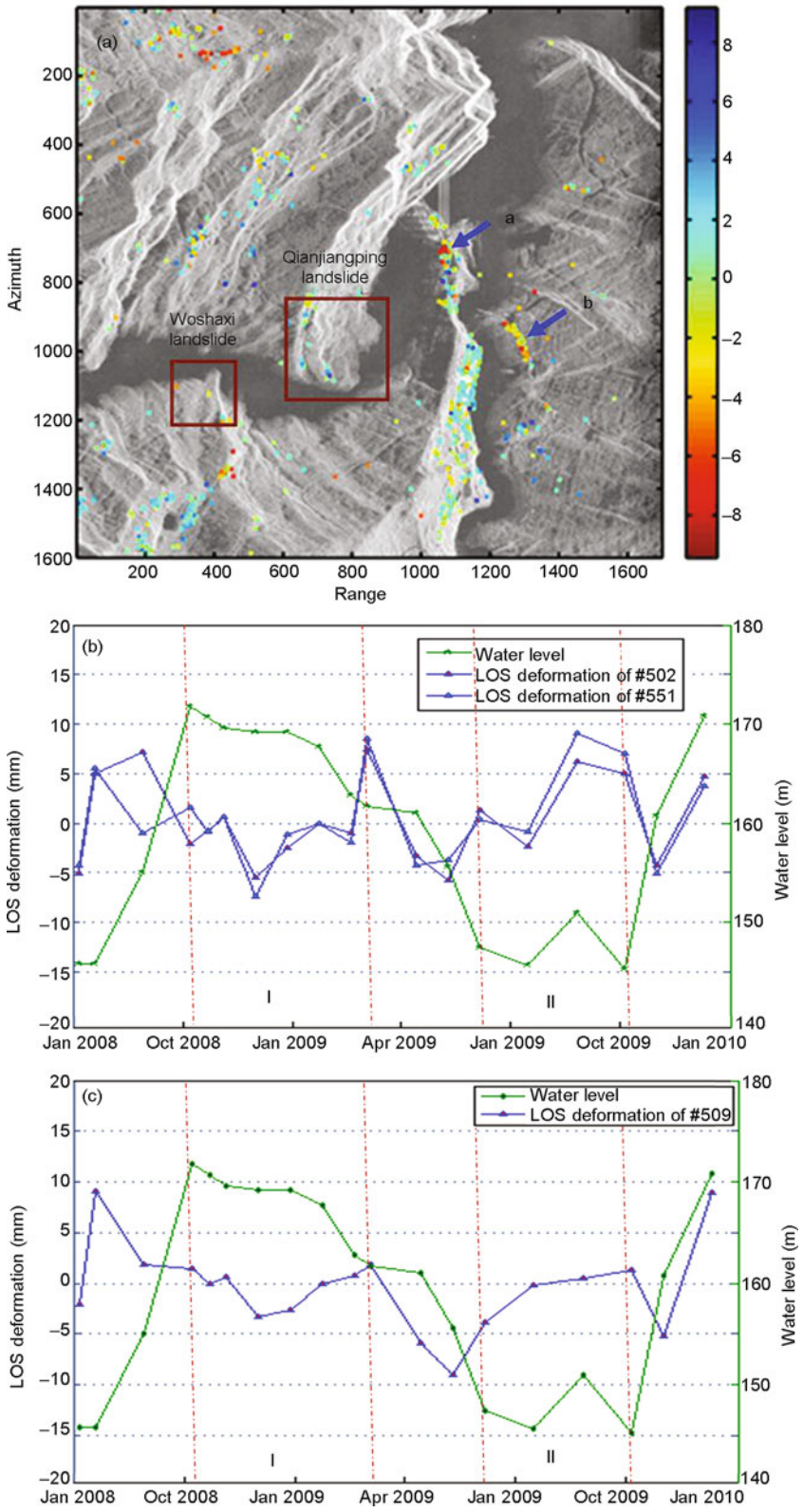

Figure 10 (a) Deformation rate of PSs in the line of sight (mm/a); (b) nonlinear deformation analysis of the Qianjiangping landslide; (c) nonlinear deformation analysis of the Woshaxi landslide.

front edge reaches the 135 m water level; the two edges are bounded with rock and earth. The base rock ridge forms western and east parts of the landslide body with average slope of 30°. The north-south length and east-west width are about 600 and 700 m respectively, while the estimated average thickness of the sliding mass is 30 m. The total estimated volume is around 1.260×10^7 m^3. The Fanjiaping landslide is also on the southern bank of the Yangtze River, upriver of the Baishuihe landslide.

The remote-sensing images of Baishuihe show a great density of plants; therefore, PSs are only detected on the back edge and the west-east border of the landslide. To describe the nonlinear deformation, two PSs on the trailing and eastern parts of the landslide are studied. In Figure 9(b), deformation of the trailing edge is not remarkable except during the period from April to June 2009, when the water level fell. Meanwhile, the eastern edge has undergone great displacement with water level changes since April 2009.

In the case of the Fanjiaping landslide, the identified PS points are mainly distributed in the area with man-made scatterers. Figure 9(c) presents the deformation series for a building. From the nonlinear trends, two types of deformation pattern are recognized: at point #2188, the displacement relates to the water level, but no trends are found, and at point #2239, the deformation has no relation with the water level but was in a state of slow downward sliding.

The Woshaxi landslide is located near Meiping, Shazhenxi, on the right bank of the Qinggan River, which is a branch of the Yangtze River. The landslide body is 1.5 km from the Qianjiangping landslide located on the left bank of the Qinggan River. The elevation of the landslide body decreases from south-west to north-east. The back edge is 405 m high and the front edge is lower than 140 m, and the volume is around 4.2×10^6 m^3. The mentioned Qianjiangping landslide is an old landslide that was a serious geological disaster in June 2003 resulting from continuous rain and impounding of the reservoir.

Figure 10(a) shows the PS deformation velocity (mm/a) along the radar sight, and Figure 10(b) shows the deformation series of a PS on the landslide body. The intervals I and II represent different periods of the Three Gorges reservoir operating with different water levels. The measured deformation during these two periods indicates that there was no obvious deformation during the high- or low-reservoir water levels. On the contrary, strong deformations are closely related to changes in water level. Therefore, more attention should be given when the water level changes notably. On the other hand, in Figure 10(a), the Qinghe bridge (as indicated by arrow a) shows an obvious deformation (8 mm/a) towards the river, which fits with a reported landslide near the Qinghe Bridge. In addition, the mountain road leading to the bridge (as indicated by arrow b) is stable with tiny deformation according to our results. On the contrary, the measured deformation suggests that the road had a large deformation trend towards the river.

4 Conclusions

There are many well-applied and reliable methods for monitoring landslide deformation; however, because of the complicated climate environment and steep terrain of the Three Gorges region, it is difficult to monitor on a large scale with highly dense and continuous measurements using such methods. The D-InSAR technique demonstrates great potential for the monitoring of ground deformation. In particular, because time-series InSAR analysis techniques overcome the limitation of decorrelation and atmospheric affects, high-precision deformation measurements can be made. Nevertheless, because of the low spatial and temporal resolution of ERS-1/2 and ASAR images, it is difficult to precisely measure landslides over the Three Gorges region.

The work presented in this paper indicates that with high-resolution TerraSAR-X data, we can identify the location, time of occurrence and deformation of a landslide by analyzing amplitude and phase information. To overcome strong decorrelation and atmospheric effects in the Three Gorges region, time-series analysis was carried out to measure the deformation series of landslide bodies. The obtained results suggest that substantial deformation did not depend on the water level of the reservoir. However, with a radical water change, abnormal deformation is observed. Comparing with TerraSAR-X and ASAR data, time series images with shorter revisiting times and higher resolution were demonstrated to obtain a denser distribution of measurement points, and thus have wider application prospects in the monitoring and prevention of geological disasters.

This work was supported by National Basic Research Program of China (Grant No. 2007CB714405), National Natural Science Foundation of China (Grant No. 41021061) and Major Research Program of the Three Gorges Region Geologic Disaster Protection (Grant No. SXKY3-6-4).

1 Ding J, Yang Z, Shang Y, et al. New prediction and warning method of landslide hazard triggered by heavy rainfall. Sci China Ser D-Earth Sci, 2006, 36: 579–586
2 Li L, the prevention and treatment of major geological disasters in Three Gorges Area. Land Resour, 2002, (4): 4–7
3 Peng X, Zhang Y, Yan D, et al. Deformation monitoring of several classic landslides after the impoundment of the Three Gorges Reservoir. In: Chinese Bureau of Geological Survey, ed. Geological Hazard Investigation and Monitoring Methods, Sept. 16–18, Beijing: China Land Press, 2004. 255–261
4 The Centre of Geology Hazards Prevention of Three Gorges Reservoir. Qianjiangping landslide in Zigui country, Hubei Province. Chin J Geol Hazard Contr, 2003, 14: 144
5 Liao M, Lin H. Synthetic Aperture Radar Interferometry-Principle and Signal Processing. Beijing: Surveying and Mapping Press, 2003. 167
6 Massonnet D, Rossi M, Carmona C. The displacement field of the

Landers earthquake mapped by interferometry. Nature, 1993, 138–142
7 Zebker H A, Rosen P A, Goldstein R M, et al. On the derivation of coseismic displacement fields using differential radar interferometry: Landers earthquake. Inter Geosci Remote Sensing Symp, 1994, 1: 286–288
8 Shan X J, Ma J, Wang C L, et al. Co-seismic ground deformation and source parameters of Mani earthquake inferred from spaceborne D-InSAR observation data. Sci China Ser D-Earth Sci, 2002, 32: 837–844
9 Fruneau B, Achache J, Delacourt C. Observation and modeling of the Saint-Etienne-de-tinee landslide using SAR Interferometry. Tectonophysics, 1996, 265: 181–190
10 Ferretti A, Prati C, Rocca F. Nonlinear subsidence rate estimation using permanent scatterers in differential SAR interferometry. IEEE Trans Geosci Remote Sensing, 2000, 38: 2202–2212
11 Ferretti A, Prati C, Rocca F. Permanent scatterers in SAR interferometry. IEEE Trans Geosci Remote Sensing, 2001, 39: 8–20
12 Best M. Kampers, Radar Interferometry Scatterer Technique. Heidberg: Springer, 2006. 43–66
13 Ferretti A, Savio G, Barzaghi R, et al. Submillimeter accuracy of InSAR time series: Experimental validation. IEEE Trans Geosci Remote Sensing, 2007, 45: 1142–1153
14 Wang Y, Liao M S, Li D R, et al. Subsidence velocity retrieval from long-term coherent targets in radar interferometric stacks. Chin J Geophys, 2007, 50: 598–604
15 Hooper A J. Persistent scatterer radar interferometry for crustal deformation. Dissertation for the Doctoral Degree. Stanford: Stanford University, 2006
16 Hooper A. A multi-temporal InSAR method incorporating both persistent scatterer and small baseline approaches. Geophys Res Lett, 2008, 35: L16302.1–L16302.5
17 Colesanti C, Ferretti A, Prati C, et al. Monitoring landslides and tectonic motions with the Permanent Scatterers Technique. Eng Geol, 2003, 68: 3–14
18 Hilley G E, Burgmann R, Ferretti A, et al. Dynamics of slow-moving landslides from permanent scatterer analysis. Science, 2004, 304: 1952–1955
19 You X, Li S,Yang S, et al. Preliminary studies on InSAR application in Three Gorges Area. Crust Deform Earthq, 2001, 21: 58–66
20 Gao L, Zen Q. Terrain deformation monitoring in Three Gorges area using permanent scatterers SAR interferometry. In: Proceedings ScanGIS'2007, 2007
21 Wang T, Perissin D, Liao M, et al. Deformation monitoring by long-term D-InSAR analysis in Three Gorges area, China. In: 2008 IEEE International Geoscience and Remote Sensing Symposium-Proceedings, July 6–11, 2008. Boston: Institute of Electrical and Electronics Engineers Inc, 2008
22 Wang T, Liao M, Perissin D. InSAR coherence-decomposition analysis. Geosci Remote Sensing Lett IEEE, 2010, 7: 156–160
23 Wang T, Perissin D, Rocca F, et al. Three Gorges Dam stability monitoring with time series InSAR analysis. Sci China Ser D-Earth Sci, 2011, 54: 720–732
24 Liao M, Tian X, Zhao Q. TerraSAR-X/TanDEM-X radar remote sensing plan and application. J Geomatics, 2007, 32: 44–46
25 Wegmuller U, Walter D, Spreckels V, et al. Nonuniform ground motion monitoring with TerraSAR-X persistent scatterer interferometry. IEEE Trans Geosci Remote Sensing, 2010, 48: 895–904
26 Baran I, Stewart M, Claessens S. A new functional model for determining minimum and maximum detectable deformation gradient resolved by satellite radar interferometry. IEEE Trans Geosci Remote Sensing, 2005, 43: 675–682
27 Zebker H A, Rosen P A, Hensley S. Atmospheric effects in interferometric synthetic aperture radar surface deformation and topographic maps. J Geophys Res, 1997, 102: 7547–7563
28 Prati C, Ferretti A, Perissin D. Recent advances on surface ground deformation measurement by means of repeated space-borne SAR observation. J Geodyn, 2010, 49: 161–170
29 Chen T. Study on Stability Evaluation of the Large-Scale Bank Landslides Under the Running of the Three Gorges Reservoir (in Chinese). Chongqing: Chongqing Jiaotong University Press, 2009. 81